Journal of Materials Chemistry A

Accepted Manuscript

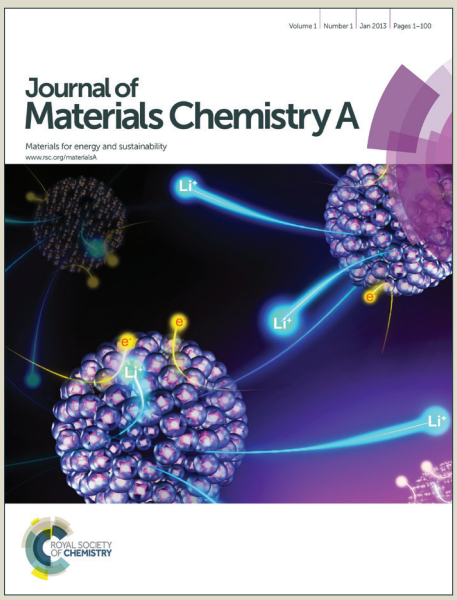

ROYAL SOCIETY OF CHEMISTRY

www.rsc.org/materialsA

Nanosized zirconium phosphate/AgCl composite materials: a new synergy for an efficient photocatalytic degradation of organic dye pollutants†

Monica Pica[a*], Morena Nocchetti[a], Berardo Ridolfi[a], Anna Donnadio[b], Ferdinando Costantino[b], Pier Luigi Gentili[b], Mario Casciola[b].

[a] *Perugia University, Department of Pharmaceutical Sciences, Via Fabretti 48, 06123 Perugia, Italy.*

[b] *Department of Chemistry, Biology and Biotechnologies, University of Perugia, Via Elce di Sotto 8, 06123 Perugia, Italy.*

[*] Corresponding author, e-mail: monica.pica@unipg.it

† **Electronic Supplementary Information (ESI) available:** it contains the temporal changes of the absorption spectrum of RhB solution in the presence of ZP, the ZP+AgCl physical mixture, ZP/*0.28* AgCl, ZP/*0.56* AgCl (Figure S1); the temporal changes of the absorption spectrum of RhB solution in the presence of ZP/*1.16* AgCl for the first, second and third cycle (Figure S2); the X-Ray powder diffraction patterns of fresh ZP/*1.16*AgCl and ZP/*1.16*AgCl after three catalytic cycles (Figure S3).

Abstract

A new class of AgCl-based composite photocatalysts has been quickly and easily obtained by using nanosized silver(I) exchanged α-zirconium phosphate as precipitating agent. Different ZP/*x*AgCl composite catalysts, having AgCl/ZP molar ratio (*x*) = 0.28, 0.56, 1.16, were prepared and characterized by X-ray diffraction analysis, scanning electron microscopy/energy dispersive X-ray spectroscopy, UV-Vis diffuse reflectance spectroscopy. The photocatalytic properties of the ZP/*x*AgCl composites, having particle size ≤ 1 μm, were investigated in the degradation of Rhodamine B, and compared with those of an AgCl sample, with particle size ranging from 0.5 to 2 μm. The ZP/*1.16*AgCl turned out to be the best photocatalyst, providing a complete chromophore structure cleavage in 15 minutes; differently, in the presence of the pure AgCl sample, the concentration of the chromophore species after 30 minutes was about half of the initial one. Moreover, the catalytic activity of ZP/*1.16*AgCl was evaluated for three consecutive catalytic tests, and an almost complete chromophore structure cleavage was achieved in 10 minutes during the third run.

1 Introduction

Layered tetravalent metal phosphates are well known materials since 1964, when crystalline zirconium(IV) phosphate was first obtained.[1] Zirconium hydrogen phosphate with a α-layered structure (α-$Zr(HPO_4)_2 \cdot H_2O$, hereafter $ZP \cdot H_2O$) is the most popular material and consists of layers made of planes of zirconium atoms bonded, on both plane sides, to monohydrogen phosphate groups. Water molecules are placed in the interlayer region, forming a hydrogen-bonding network with the phosphate groups. Small monovalent and divalent cations, such as Li^+, Na^+, Ag^+, Tl^+, Cu^+, Ca^{2+}, are able to exchange the protons of microcrystalline $ZP \cdot H_2O$ at a high rate.[1] On this regard, it was found that the affinity of $ZP \cdot H_2O$ for silver ion is greater than for any alkali metal cation.[2] This fact suggested that silver exchanged ZP could be used as source of Ag^+ ions for the precipitation of insoluble silver salts, such as silver halides AgX (X= Cl, Br, I). In recent years, silver halide materials received increasing attention owing to their light–driven catalytic performances in the degradation of organic pollutants.[3] In particular, heterojunctions based on silver halide semiconductors and silver nanoparticles (AgNPs) turned out to be efficient and promising photocatalysts under visible light.[4] It was proved that metallic AgNPs formed on the surface of AgX (Ag@AgX) act as a kind of sensitizer, enhancing the visible light absorption of the photocatalysts, because of their size- and shape-dependent plasmon resonance,[5] which speeds up the separation process of the photogenerated electrons and holes in the semiconductor catalyst.[5-6] Moreover, it was also demonstrated that AgNPs in Ag@AgCl hinder the combination of the photogenerated electrons with Ag^+ ions, and allow the formation of elemental Cl· species (by combining Cl^- ions with photogenerated holes) which oxidize the organic pollutants efficiently.[5]

In the present paper new AgCl-based composite catalysts has been quickly and easily obtained by treatment of nanosized silver exchanged α-zirconium phosphate ($ZP \cdot Ag_x$) with HCl. The ZP/*x*AgCl composite catalysts, with AgCl/ZP molar ratios, x = 0.28, 0.56, 1.16, were characterized by X-ray diffraction analysis, scanning electron microscopy/energy dispersive X-ray spectroscopy

(SEM/EDX), UV-Vis diffuse reflectance spectroscopy. The photocatalytic properties of the ZP/*x*AgCl composite catalysts were investigated in the degradation of Rhodamine B, which was chosen as pollutant model, under irradiation with a halogen lamp. Moreover, the catalytic activity of the best composite photocatalyst was also evaluated under three consecutive tests.

2 Experimental

2.1 Materials

Zirconyl propionate ($ZrO_{1.26}(C_2H_5COO)_{1.49}$, MW=220 Da) was supplied by MEL Chemicals, UK. Concentrated orthophosphoric acid (85%, 14.8 M) was purchased from Fluka, and anhydrous propanol was from Carlo Erba. All other reagents were from Aldrich and used without further purification.

2.2 Synthesis of nanocrystalline ZP.

Nanocrystalline ZP (hereafter ZP) was prepared according to ref. 7. Specifically, 3.3 mmol of zirconyl propionate were dissolved in 10 mL of anhydrous propanol. Concentrated phosphoric acid was added, at room temperature under stirring, to the above solution so that the H_3PO_4/Zr molar ratio was 6. The obtained clear mixture turned into a semitransparent gel in few minutes. The gel was first washed with propanol and then dried in oven at 60°C for 15 hours. The obtained ZP powder was washed with 10^{-3} M HCl and dried at 60°C. The P/Zr molar ratio, determined by ICP analysis, was around 2.

2.3 Preparation of AgCl and ZP/AgCl composite catalysts.

1 g of nanocrystalline ZP was suspended in water and a suitable volume of a $5 \cdot 10^{-2}$ M silver acetate solution was added to the ZP suspension so that the $[Ag^+]$ was $1.2 \cdot 10^{-2}$ M in all experiments, while the Ag/Zr molar ratio (hereafter R) was 0.3, 0.6, 1.2. The mixture was left under stirring in the dark at room temperature for five hours, so as to promote the H^+/Ag^+ exchange, and then centrifuged.

The recovered solid, sheltered from light, was quickly washed with water and dried at room temperature over P_2O_5. The P/Zr molar ratio, determined by ICP analysis, was around 2 for all materials, so that the general composition $ZrAg_xH_{2-x}(PO_4)_2$ (hereafter indicated as ZP·Ag_x) can be assumed. The ZP·Ag_x materials were first washed with an excess of 0.5 M HCl (Cl/Ag molar ratio ≈ 30) and then with 10^{-3} M HCl, so as to promote the precipitation of AgCl in the presence of the ZP particles. The solids, hereafter indicated as ZP/*x*AgCl, were then dried at room temperature over P_2O_5.

Pure AgCl, to be used as reference material, was prepared by adding an excess of 0.5 M HCl (Cl/Ag molar ratio ≈ 30) to a $5 \cdot 10^{-2}$ M silver acetate solution; the solid was then washed with 10^{-3} M HCl and finally dried at room temperature over P_2O_5. All materials were sheltered from light before the catalytic tests.

2.4 Photocatalytic degradation of Rhodamine B

The photocatalytic degradation of Rhodamine B (RhB) dye was carried out by suspending a weighted amount of ZP/*x*AgCl or pure AgCl in 25 mL of a 10^{-5} M RhB dye solution. The catalyst amounts employed for the photocatalytic experiments, expressed as (mg AgCl/mL RhB), were reported in Table 2. Before experiments, the mixtures were kept in the dark for 30 minutes under magnetic stirring to reach the adsorption–desorption equilibrium. Then, they were irradiated with a 105 W Osram halogen lamp with a UV filter (providing radiation with $\lambda \geq 350$ nm): the UV light accounts for less than 2% of the visible light. The sample illumination area was 16 cm^2 and the distance between the light source and the upper surface of the liquid was 7.5 cm. At given intervals of irradiation time, about 3 mL of suspension was taken, under stirring, from the reaction vessel, centrifuged and analysed by UV-Vis absorption spectroscopy, in order to follow the RhB photodegradation during time. A similar experiment was carried out also with pure ZP. For each composition of the photocatalyst, three degradation tests were carried out by using samples of three photocatalyst batches.

2.5 Techniques

X-ray diffraction patterns were collected with a Philips X'Pert PRO MPD diffractometer operating at 40 kV and 40 mA, with a step size 0.0167° and 50 s counting time, using Cu Kα radiation and an X'Celerator detector.

Scanning electron microscopy (SEM) images were collected by a Zeiss LEO 1525 FE SEM, at the LUNA Laboratory of the Department of Physics and Geology of Perugia University. The powder samples were suspended in water and dropped on an aluminum stub precoated with a double sided adhesive conductive carbon tape. Then, the samples were coated with a thin layer of chromium before SEM analysis.

The (P/Zr) molar ratio and the Ag content of all the ZP·Ag_x samples was determined by using an ICP Varian Liberty inductively coupled plasma-optical emission spectrometer (ICP-OES) with axial injection. A weighed amount of the samples was dissolved in 3 M HF (≈ 2 mL) and then diluted with water.

The RhB absorption spectra were carried out by a UV-Vis Agilent Model 8453 Spectrophotometer, using a quartz cell of 1 cm path length. The spectra were recorded at room temperature within the range 200–900 nm.

Reflection measurements have been carried out by using a portable spectrophotometer composed of Avantes parts and a deuterium-halogen lamp (AvaLight-DH-2000-FHS). An integrating sphere with a 6 mm diameter viewing aperture and 88 irradiation angle (ISP-30-6) has been used to collect and transfer the reflectance signals to an AvaSpec–2048 charge-coupled device (CCD) detector via a quartz fiber-optic system (diameter 600 μm). The AvaSoft software controls the acquisition of the spectra in the 200 to 1100 nm range. The reflectance spectra have been recorded before and after irradiating the samples through the same halogen lamp used for the catalytic experiments. The experimental reflectance values R have been normalized to 1 and transformed in ratios of the absorption (K) and scattering (S) coefficients through the following algorithm:

$$\frac{K}{S} = \frac{(1-R)^2}{2R}$$

in agreement with the Kubelka-Munk theory.[8]

3 Results and discussion

3.1 Structural characterization

The H^+/Ag^+ ion exchange reaction in α-type ZP was thoroughly studied by Costantino *et al.*[9]: in their study, microcrystalline ZP was equilibrated with silver acetate solutions at room temperature and the presence of the Brönsted base, CH_3COO^-, kept the pH of the solution high enough to assure an almost quantitative H^+/Ag^+ exchange. Moreover, it was also found that the dihydrogen phase is directly transformed into the fully exchanged phase, $Zr(AgPO_4)_2$, having an interlayer distance of 7.78 Å in the absence of interlayer water molecules.

In the present work, silver exchanged ZP samples were prepared by contacting aqueous suspensions of nanocrystalline ZP with suitable volumes of a silver acetate solution, giving a Ag/Zr molar ratio (R) of 0.3, 0.6, 1.2.

The Ag/Zr molar ratio (hereafter *x*), determined by ICP analysis, was 0.28, 0.57 and 1.16 for R= 0.3, 0.6, 1.2, respectively. For the sake of simplicity, the composition of the exchanged materials will be hereafter indicated as $ZP{\cdot}Ag_x$. It can be observed that the *x* values differ from the R values by 7%, at maximum, so that the H^+/Ag^+ exchange can be considered quantitative also for nanosized ZP.

The X-ray diffraction patterns of the $ZP{\cdot}Ag_x$ samples and pristine ZP are reported in Figure 1. The peaks of pattern (a), at 11.69°, 19.77°, 24.96°, 33.81° 2θ are respectively assigned to the (002), (110), (112), (020) crystallographic planes of the α-$ZP{\cdot}H_2O$ phase. For $x \leq 0.28$, no significant differences were observed between the patterns of $ZP{\cdot}Ag_x$ and ZP, suggesting that in these conditions the Ag^+ uptake mainly occurs on the particle surface.

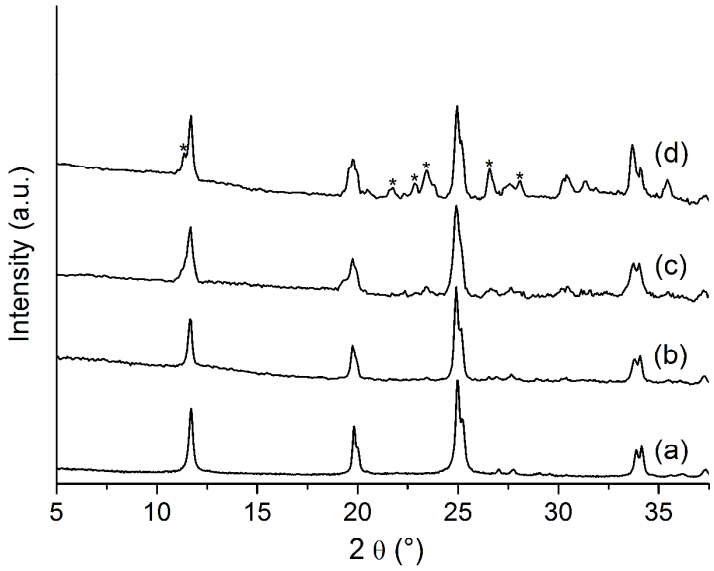

Figure 1. X-Ray powder diffraction patterns of ZP (a), ZP·$Ag_{0.28}$ (b), ZP·$Ag_{0.56}$ (c), ZP·$Ag_{1.16}$ (d). The peaks labelled with asterisks refer to the $Zr(AgPO_4)_2$ phase.

When the *x* value reaches 0.56, the peak at 11.69° 2θ broadens, while for x=1.16 the main peaks of the fully exchanged anhydrous phase, having composition $Zr(AgPO_4)_2$, appeared, besides those typical of α-ZP·H_2O phase.

The treatment of the ZP·Ag_x samples with hydrochloric acid was expected to provoke the precipitation of silver chloride and the concomitant regeneration of the hydrogen form of ZP, according to the reaction:

$$ZP{\cdot}Ag_x \xrightarrow{HCl} ZP + x\,AgCl$$

The materials obtained after treatment of ZP·Ag_x with hydrochloric acid will be hereafter indicated as ZP/*x*AgCl.

Both the ZP/*x*AgCl composites and the AgCl sample used as reference material were studied in terms of combined structural and microstructural characterization, by using the Rietveld method implemented in the GSAS-EXPGUI crystallographic suite.[10] Figure 2 reports the Rietveld plot for the ZP/*x*AgCl composites, showing the observed and calculated profiles and their difference. As

expected, the typical peaks of α-ZP·H_2O are observed in all patterns. The main peaks at 27.85°, 32.21°, 46.28° 2θ are the (111), (200) and (220) reflections of the AgCl cubic phase. Moreover, the reflections of the $Zr(AgPO_4)_2$ phase, observed in pattern d) of Figure 1, are missing after treatment of ZP·$Ag_{1.16}$ with HCl, so that the Ag^+/H^+ exchange can be considered almost complete, even at high Ag^+ loadings. Both size and strain contributions to the line broadening of the AgCl and ZP peaks were considered and the corresponding Gaussian and Lorentzian factors were refined by using a modified Pseudo-Voigt function (profile function no. 3 in GSAS). First, the instrumental contribution to the peak broadening was previously evaluated by the Rietveld refinement of the profile of lanthanum hexaboride, LaB_6, as an external peak profile standard. We assumed that the standard was not affected by microstrain, and the instrumental broadening was modeled by the refinement of W and Y peak shape parameters for Gaussian and Lorentzian contributions, respectively. It should be noted that the full width at half maximum (FWHM) of the main peaks of the AgCl was close to the instrumental broadening function, thus suggesting a large domain size for the AgCl particles (>200 nm) whereas those corresponding to ZP had wider FWHM corresponding to lower crystalline domain sizes (<200 nm). The refined peak shape parameters were P, X, and Xe, accounting for Gaussian and Lorentzian contributions to size effects, and U, Y, and Ye for the corresponding microstrain effects, whereas W was fixed at the value refined on the standard. Two additional parameters for modeling asymmetry at low angle were also refined. Coherent domain size (volume weighted) parallel and perpendicular to different broadening axes was calculated. For AgCl the (200) broadening axis was considered for the evaluation of size effects on the line broadening dependent to these direction whereas for ZP the (001) directions was chosen. $D_{\parallel}$ and $D_{\perp}$ to the selected broadening axes were calculated by using the following formulas:

$D_{\parallel} = 1800\lambda/\pi(X + Xe)$ and

$D_{\perp} = 1800\lambda/\pi X$.

Moreover, the relative phase amount, expressed as weight phase fraction percentage, of the ZP/*x*AgCl composites was evaluated by using the Bish and Howard formula:[11]

$$W_m = \frac{a_m S_m}{\sum_{k=1}^{k=m} a_k S_k}$$

where W_m and a_k are the weight fraction of the mth component in the sample and its calculated density, respectively; a_k is given as follows: $a_k = Z_k M_k U_k$ where Z_k, M_k, and U_k are the number of chemical formula units in a unit cell, the molecular weight, and the unit-cell volume, respectively.

The results of the Rietveld refinement, the coherent domain sizes and the quantitative phase analysis for all the examined samples are reported in Table 1.

Table 1. Refinement details and microstructural parameters for pure AgCl and for the ZP/*x*AgCl composites.

		x= 0.28	*x= 0.56*	*x= 1.16*	*Pure AgCl*
wRp		0.058	0.056	0.054	0.066
Rp		0.044	0.043	0.042	0.052
RF^2		0.13	0.10	0.11	0.04
GOF		1.46	1.47	1.36	1.34
AgCl	D∥200	271 nm	329 nm	293 nm	496 nm
	D⊥200	294 nm	274 nm	346 nm	437 nm
ZP	D∥001	42 nm	45 nm	30 nm	
	D⊥001	63.5 nm	72 nm	61 nm	
ZP/AgCl weight ratio		83.9/16.1	71.2/28.8	66.4/33.6	
		86.1/13.9[a]	71.2/28.8[a]	41.5/58.5[a]	

[a] Calculated on the basis of the Ag/Zr molar ratio in ZP·Ag_x, determined by ICP analysis.

As a matter of fact, the average crystalline size of AgCl crystals, measured along and perpendicularly to the *a*-axis, looks to be almost isotropic, according to the cubic symmetry. In addition, they result to be about 5 times larger than that of ZP. Moreover, the crystalline domain size of AgCl in the composites increases with increasing the *x* value but results to be, on the whole,

smaller than that of pure AgCl. The domain size of the pure AgCl is very large (> 400nm) and the corresponding FWHM is close to the instrumental broadening, therefore its contribution to the whole broadening is so small that it cannot be accurately evaluated.

The ZP/AgCl weight ratio for ZP/*0.28*AgCl and ZP/*0.56*AgCl, calculated by X-ray analysis, resulted to be in quite good agreement with that calculated from the Ag/Zr molar ratio in the corresponding ZP·Ag_x precursors: this fact suggests that both phases are highly crystalline in those composites.

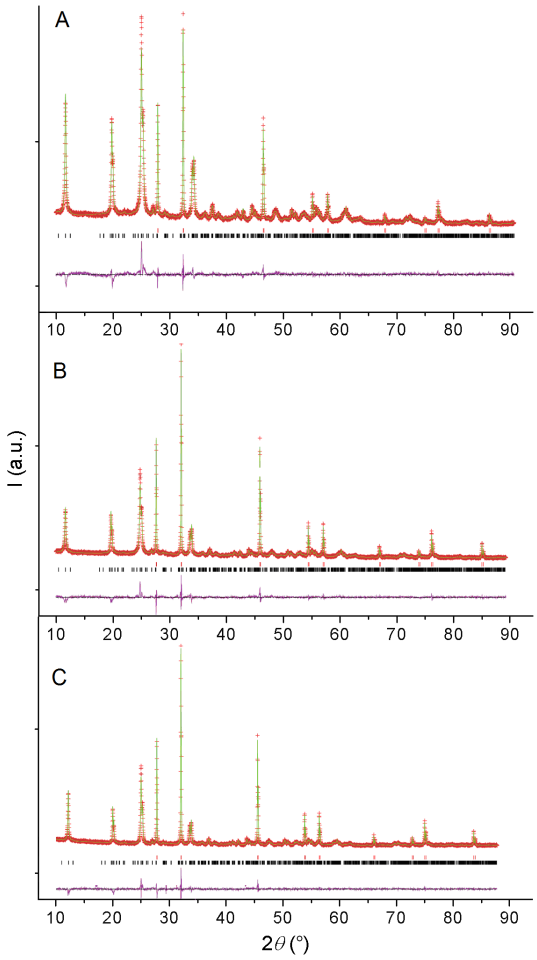

Figure 2. Rietveld plot of the last cycle of refinement for ZP/*0.28*AgCl (A), ZP/*0.56*AgCl (B), ZP/*1.16*AgCl (C), showing the observed (red) and calculated (green) profiles and their difference (blue). Red marks indicate calculated positions of Bragg peaks of AgCl; black marks those of ZP.

Differently, the ZP/AgCl weight ratio for ZP/*1.16*AgCl, estimated from X-ray analysis, is quite different from that calculated by ICP analysis on ZP·$Ag_{1.16}$; by taking into account that the Ag/Zr atomic ratio for ZP/*1.16*AgCl, determined by EDX analysis, is in good agreement with that found by ICP analysis (1.20 *vs.* 1.16), the above difference could be ascribed to the presence of amorphous AgCl which cannot be evaluated by X-ray diffraction analysis.

3.2 SEM analysis

Figure 3a shows the SEM image of the pure AgCl sample, used as reference material: it consists of particles having a not well defined morphology, with size in the range 0.5-2 μm and, in general, larger than that estimated for the crystalline domain size by X-ray analysis; some of these particles are fused together, thus forming larger micrometric aggregates. Moreover, the surface of some particles is decorated by smaller spherical particles: it is well known that AgCl is unstable under light exposition and it is reasonable to infer that those smaller particles consist of metallic silver obtained by reduction of AgCl during the SEM analysis and accidental daylight exposition of the material. The ZP sample (Figure 3b) consists of flat nanoparticles with an irregular shape and planar size in the range 50-500 nm. The SEM images of the ZP/*x*AgCl composite materials are reported in Figures 3c-f. At first sight, the AgCl particles are not clearly distinguishable; however, a careful examination of the SEM images, collected at low magnification, revealed the presence of some almost cubic-shaped particles, embedded between the ZP nanoplatelets (see for example the red circles and Figure 3f), having size ≤ 1 μm; they can be reasonably identified as AgCl particles. The EDX mapping, of the area of the ZP/*1.16* AgCl sample reported in Figure 4a, revealed that the Ag and Cl elements are effectively localized in the same regions, having size similar to those estimated from Figure 3e. From the SEM analysis it can be reasonably inferred that the AgCl particles in the ZP/*x*AgCl composite are, on the whole, smaller than those of the pure sample, suggesting that when ZP·Ag_x is used as source of Ag^+ ions for the precipitation of AgCl, instead of silver acetate, the particle growth and aggregation is reduced to some extent.

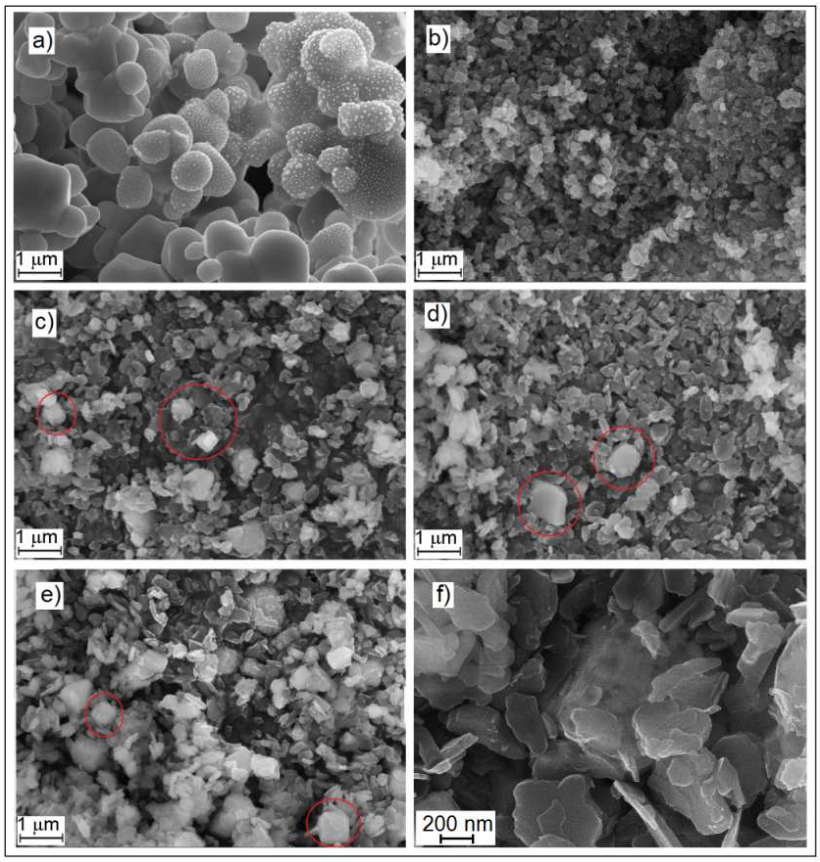

Figure 3. Representative SEM images of pure AgCl (a); pure ZP (b); ZP/*0.28*AgCl (c); ZP/*0.56*AgCl (d); ZP/*1.16* AgCl (e and f)

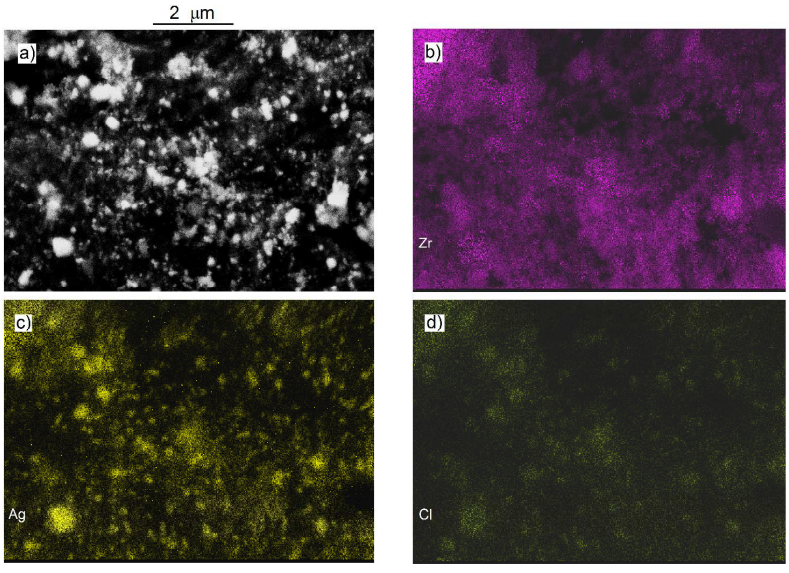

Figure 4. SEM image of ZP/*1.16* AgCl (a); EDX mapping images of the ZP/*1.16* AgCl composite (b-d).

3.3 Photochemical characterization.

Figure 5 and 6 show the absorption spectra, in Kubelka–Munk units,[8] of AgCl and ZP/*1.16*AgCl, respectively, before and after 3 minutes of irradiation with the same halogen lamp used for the photocatalytic tests (providing radiation with $\lambda \geq 350$ nm): K and S are the absorption and the scattering coefficients, respectively. Figure 6 also shows the absorption spectrum of ZP (curve a), which did not change after irradiation. Before irradiation, both pure AgCl and ZP/*1.16*AgCl show an absorption band below 400 nm which can be ascribed to the characteristic absorption of the AgCl semiconductor; it should be also observed that the intensity of this absorption band is lower for ZP/*1.16*AgCl than for pure AgCl, due to the presence of ZP which exhibited a very low K/S ratio.

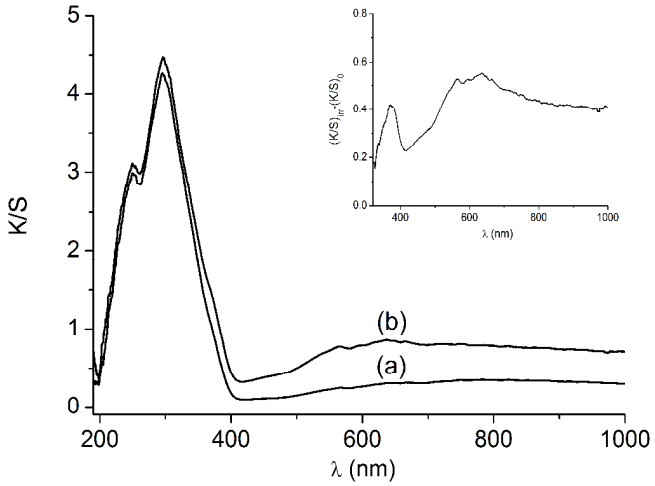

Figure 5. Absorption spectra in terms of the Kubelka–Munk function[8] (K/S) of pure AgCl before irradiation (a) and after 3 minutes of irradiation (b); Inset: spectrum calculated as difference between (b) and (a) spectra.

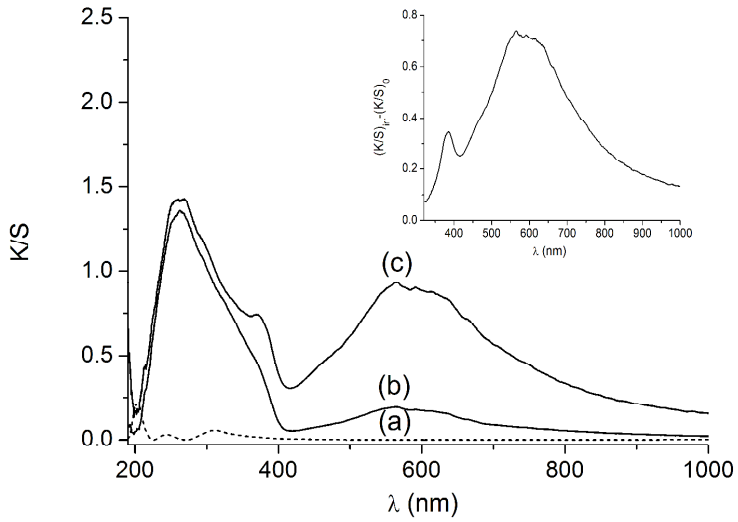

Figure 6. Absorption spectra in terms of the Kubelka–Munk function[8] (K/S) of ZP before and after irradiation (a), ZP/*1.16*AgCl before irradiation (b) and after 3 minutes of irradiation (c). Inset: spectrum calculated as difference between (c) and (b) spectra.

The small absorptions in the visible region, before irradiation, are due to tiny amounts of silver produced by the environmental light during the synthesis of the materials. Such bands in the visible region are due to the surface plasmon resonance of silver nanoparticles formed by reduction of the Ag(I) ions of the AgCl lattice by light.[12] It was observed that both materials became gradually grey –mauve just after few seconds of focused irradiation and an appreciable increase of the absorption in the visible region was observed after 3 minutes of irradiation: these two facts support the effective formation, under the employed irradiation conditions, of the Ag nanoparticles.[13] Actually, it is known that AgCl absorbs UV light and it is reasonable that the Ag^+ ions of the AgCl lattice can undergo reduction upon irradiation with the halogen lamp exhibiting a low content of UV radiation (less than 2% of the visible light), thus forming metallic silver on the AgCl surface.

It is also interesting to observe that the absorption bands of AgCl and ZP/*1.16*AgCl in the visible region are significantly different. This appears more evident if one considers the difference spectra (see insets of Figure 5 and 6). In particular, the difference spectrum of ZP/*1.16*AgCl exhibited an almost symmetric absorption band between 420 and 800 nm with a maximum around 565 nm,

while that of AgCl showed a broader and asymmetric band at λ >420 nm, with a maximum around 635 nm.

It is well known that the spectral position of the plasmonic absorption of metal nanoparticles depends on their shape, size, mutual distance, and surrounding materials.[12,14-15] Moreover, it has been demonstrated that large particles size and short separation distances of metal nanoparticles cause a red-shift in surface plasmon resonance absorption spectra.[14, 15] In light of these facts, it can be inferred that AgCl and ZP/*x*AgCl are effectively converted, after few minutes of irradiation, in Ag@AgCl and ZP/*x*(Ag@AgCl), respectively, thus extending the light response of AgCl into the visible light region. Moreover, the presence of ZP seems to affect the formation of the silver nanoparticles by irradiation, in terms of size distribution and particle aggregation. The band broadening, at λ>400 nm, and the red-shift of λ_{max} observed for pure AgCl, with respect to ZP/*x*AgCl, let us suppose that silver nanoparticles in Ag@AgCl may be characterized by a larger size and/or a shorter interparticle distance.

3.4 Photocatalytic performance of ZP/*x*AgCl

The photocatalytic performances of the ZP/*x*AgCl composites were tested in the degradation process of Rhodamine B (RhB) under irradiation with a halogen lamp, providing radiation with λ≥ 350 nm. The particles of the freshly prepared photocatalysts were suspended in 25 mL of a 10^{-5} M RhB solution and left under stirring in the dark for 30 minutes in order to reach the equilibrium for the adsorption of the dye. The catalyst's amount used in each experiment, expressed as (mg photocatalyst/mL RhB) and (mg AgCl/mL RhB), was reported in Table 2.

Then, the mixtures were irradiated and the RhB concentration was followed by spectrophotometric analysis. For comparison, additional experiments were carried out with pure ZP, pure AgCl and a physical mixture of ZP and AgCl with the same composition used for Exp. N° II.

Table 2. Amount of pure AgCl, ZP/*x*AgCl and ZP catalyst used for the catalytic experiments.

Sample	*Exp. N°*	*mg photocatalyst/mL RhB*	*mg AgCl/mL RhB*
AgCl	I	0.74	0.74
ZP/*1.16*AgCl	II	2	0.74
ZP/*0.56*AgCl	V	2	0.45
ZP/*0.28*AgCl	VI	2	0.24
ZP	VII	1.3	
ZP+AgCl physical mixture	VIII	2	0.74

As an example, Figure 7 shows the temporal evolution of the RhB absorption spectrum under irradiation for the kinetic experiments carried out with pure AgCl (*Exp. N°* I) and ZP/*1.16*AgCl (*Exp. N°* II). The temporal evolution of the absorption spectrum of RhB in all other experiments was reported in Figure S1. The typical absorption spectrum of RhB shows a main peak at 554 nm; the molar extinction coefficient of RhB at 554 nm (hereafter indicated as ε_0) is 11.5 x 10^4 M^{-1} cm^{-1}.[16] The absorption spectra before irradiation show in all cases a decrease of the absorbance at 554 nm, with respect to that of the RhB solution before adding the catalyst: this decrease can be attributed to the adsorption of RhB molecules on the solid particles. Moreover, except for the kinetic experiment carried out with pure ZP (Figure S1), irradiation in the presence of all photocatalysts causes a further and significant decrease in the absorbance of RhB during time, with a concomitant blue shift of the wavelength of the absorption maximum, λ_{max} (Figures 7 and S1). As reported in the literature,[16] the observed blue-shift of λ_{max} is due to the RhB de-ethylation, occurring on the catalyst surface[17] in a stepwise manner, which can lead to the formation of N,N,N'-triethylated Rhodamine (λ_{max} = 539 nm, ε_{539}=5.5 x 10^4 M^{-1} cm^{-1}), N,N'- diethylated Rhodamine (λ_{max} = 522 nm, ε_{522}=7.2 x 10^4 M^{-1} cm^{-1}), N-ethylated Rhodamine (λ_{max} = 510 nm, ε_{510}=6.1 x 10^4 M^{-1} cm^{-1}), and finally Rhodamine (Rh, λ_{max} = 497 nm, ε_{497}=8.4 x 10^4 M^{-1} cm^{-1}).[16]

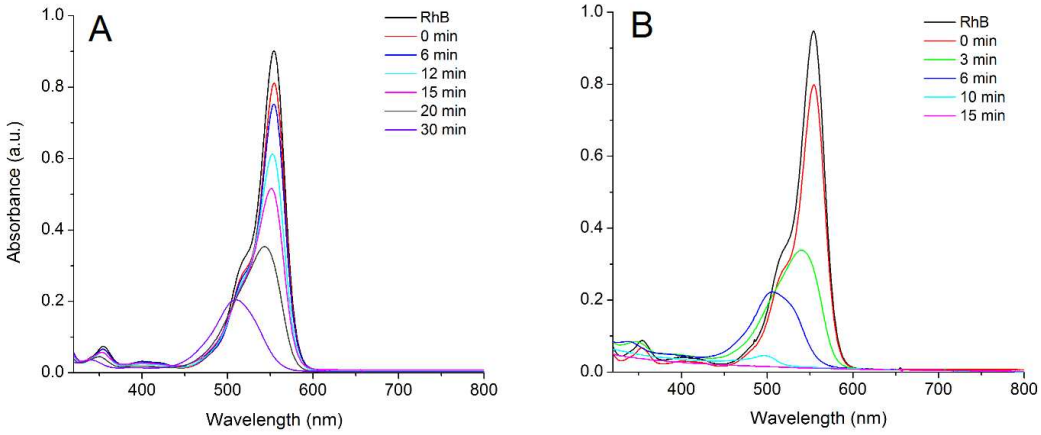

Figure 7. Temporal changes of the absorption spectrum of the RhB solution in the presence of the following amounts of photocatalyst per RhB mL: 0.74 mg of AgCl (A); 2 mg of ZP/*1.16*AgCl (B).

The values of the λ_{max} shift ($\Delta\lambda_{max}$) as function of the irradiation time were reported in Figure 8. It can be observed that the de-ethylation process depends on the kind of photocatalyst. In particular, it was observed that RhB is completely de-ethylated within 10, 15, 20 minutes in the presence of ZP/*1.16*AgCl, ZP/*0.56*AgCl, ZP/*0.28*AgCl, respectively (Figure 8B), while it is converted in N-ethylated Rhodamine in 30 minutes, in the presence of pure AgCl. Surprisingly, if the catalytic process is carried out with the physical mixture, the de-ethylation process is almost complete in 30 min. It is also noteworthy that in the presence of ZP/*1.16*AgCl, ZP/*0.56*AgCl, ZP/*0.28*AgCl, the absorbance in the visible region, due to the conjugated chromophore structure of RhB, goes to zero in at most 15, 20 and 30 min, respectively.

The analysis of a kinetic experiment requires the calculation of the relative concentration of a reactant as a function of time. This calculation is not trivial in the present work, because irradiation of RhB in the presence of the photocatalysts resulted in both chromophore structure cleavage and de-ethylation reaction, so that both residual RhB and its de-ethylated species can coexist, especially at the early stages of the catalytic reaction.

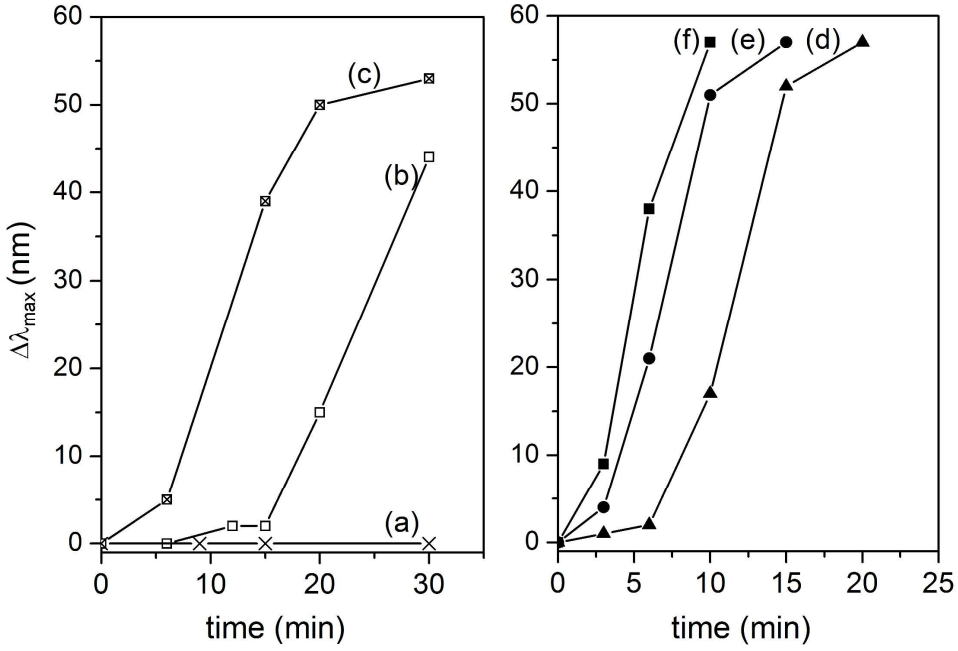

Figure 8. Wavelength shift of the maximum value of the absorbance ($\Delta\lambda_{max}$) of the RhB solution as function of time in the presence of the following amounts of photocatalyst per RhB mL: 1.3 mg of pure ZP (a), 0.74 mg of pure AgCl (b), 2 mg of the ZP+AgCl physical mixture (c); 2 mg of ZP/*0.28*AgCl (d), ZP/*0.56*AgCl (e), ZP/*1.16*AgCl (f).

Therefore, if the absorption spectra of the de-ethylated species were known, the relative concentration of the different dye species, formed during irradiation, should be calculated by deconvolution of the spectra of Figures 7 and S1. However, it is possible to estimate the relative concentration of RhB as function of time from the absorbance at 554 nm, by applying the Lambert-Beer law:

$$\frac{C_{RhB}}{C_0} = \frac{A}{A_0}$$

where C_{RhB} is the concentration of RhB at a given time *t*; C_0 is the concentration of RhB before irradiation (and after equilibration of the RhB solution with the photocatalyst); A is the absorbance at 554 nm at time *t*; A_0 is the absorbance at 554 nm before irradiation (and after equilibration of the RhB solution with the photocatalyst). The C_{RhB}/C_0 values as function of time are shown in Figure 9,

and refer to the average values, obtained by three different catalytic experiments, with a 10% of maximum uncertainty. It should be considered that the above equation provides overestimation of the RhB relative concentration, since the absorption bands of the de-ethylated species formed during irradiation are overlapped with that of residual RhB, thus contributing to the measured absorbance value at 554 nm.

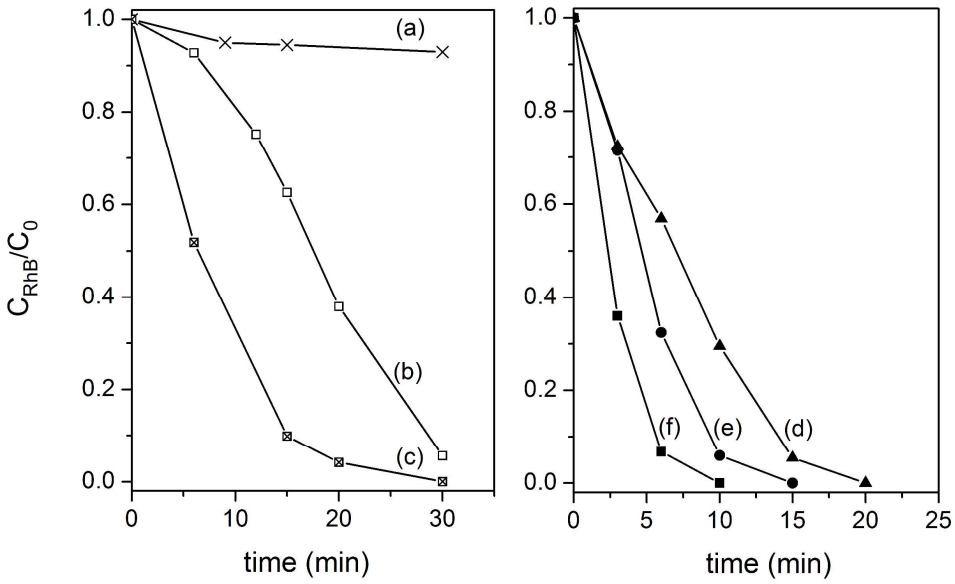

Figure 9. Relative concentration, C_{RhB}/C_0, of RhB as a function of the irradiation time, in the presence of the following amounts of photocatalyst per RhB mL: 1.3 mg of pure ZP (a), 0.74 mg of pure AgCl (b), 2 mg of the ZP+AgCl physical mixture (c); 2 mg of ZP/*0.28*AgCl (d), ZP/*0.56*AgCl (e), ZP/*1.16*AgCl (f).

It can be observed that all composites are more efficient than the pure AgCl sample, leading to a complete disappearance of RhB in at most 10, 15 and 20 min in the presence of ZP/*1.16*AgCl, ZP/*0.56*AgCl, ZP/*0.28*AgCl, respectively. Again, the physical mixture exhibited a better performance than the pure AgCl sample. In order to evaluate if the complete disappearance of RhB in the presence of the composites is due to both de-ethylation and chromophore structure cleavage, one should take into account that the ratio between the molar extinction coefficient of RhB at 554 nm and that of Rh at 497 nm is 0.73. As a consequence, if the complete de-ethylation occurred

without the chromophore degradation, the corresponding ratio between the absorbance maximum of Rh at 497 nm and A_0 should be 0.73. Actually, the absorbance ratios calculated at 10, 15 and 20 min in the presence of ZP/*1.16*AgCl, ZP/*1.16*AgCl, ZP/*0.28*AgCl, respectively, resulted to be lower than the above value, suggesting that the chromophore structure cleavage occurred together with de-ethylation. The percentage of chromophore degradation was then estimated and reported in Table 3.

Table 3. Percentage of chromophore cleavage achieved with the indicated catalysts.

Sample	*mg photocatalyst/mL RhB*	*% chromophore cleavage*	*Time (min)*
AgCl	0.74	57±5	30
ZP/*1.16*AgCl	2	92±5 (cycle 1)	10
		93±6 (cycle 2)	10
		95±5 (cycle 3)	10
ZP/*0.56*AgCl	2	86±6	15
ZP/*0.28*AgCl	2	64±6	20
ZP	1.3		
ZP+AgCl physical mixture	2	69±5	30

The above results clearly show that :

- the ZP/*x*AgCl composites exhibit better catalytic properties than both pure AgCl and the physical mixture; the ZP/*1.16*AgCl resulted to be the best photocatalyst;

-the physical mixture works better than the pure AgCl sample, especially toward the de-ethylation process of RhB.

Due to the complexity of the investigated systems, it is not trivial to understand all the processes involved in the photocatalytic reaction. However, the literature data were very helpful on this regard and allow us to speculate about the possible roles of ZP.

First, it was already observed that the AgCl particles and/or particle aggregates precipitated from ZP·Ag_x are smaller than those precipitated from CH_3COOAg. As a matter of fact, it is known that, by decreasing the particle size the surface-to-volume ratio increases, thus increasing the number of catalytic active sites.[18]

Also, the Ag nanoparticles formed upon irradiation of the composites resulted to be smaller and/or less aggregated than those obtained by irradiation of the pure AgCl sample, thus providing a better interface contact with the AgCl matrix. On this regard, it is known that the excitation of the surface plasmon resonance of the Ag nanoparticles by the visible light, (provided in our case by the halogen lamp) enables the electron transfer from the metal to AgCl during the decay of the surface plasmon resonance.[5b] As a result, a wide-band gap semiconductor that is originally inactive under visible light obtains extra electrons, which can thereafter perform catalytic reduction reactions. The holes left behind in the metal nanocrystals have a mild oxidation ability, which can be utilized for oxidation of organic molecules.[5b]

In light of this, it is reasonable to infer that the better interface between Ag nanoparticles and AgCl particles in the ZP/*x*(Ag@AgCl) composites, facilitates the interfacial electron transfer, promotes charge carrier separation, and, consequently the photocatalytic activity.

Secondly, another factor that might be responsible for the better catalytic properties of the composites photocatalysts and of the physical mixture, in comparison with the pure AgCl sample, is the ability of ZP to chemisorb RhB. As reported by Merka et al.,[17c] the chemisorption of RhB onto the surface of silica particles, via the positively charged diethylamino group, enables the electron injection from the dye into the conduction band of the semiconductor, thus generating the radical cation $RhB^{\bullet+}$ under visible light illumination. Moreover, the injected electron reacts with adsorbed oxidants, usually O_2, to produce reactive oxygen radicals. The de-ethylation process occurs by reaction of the radical cation $RhB^{\bullet+}$ with the reactive oxygen radicals and/or molecular oxygen.[17c] A similar process is expected to occur on the surface of layered α-ZP. As a matter of fact, α-ZP is a well known material with a strong affinity for cationic dyes such as RhB, methylene blue and crystal violet,[19] which are chemisorbed on the surface through an ion-exchange reaction, involving a protonated diethylamino group of the dye and the –POH group of the ZP surface.

On the basis of these considerations, it's likely that, when ZP is in contact with AgCl, the chemisorption of RhB onto ZP could enable the electron injection from the electronically excited

dye in the conduction band of the adjoining AgCl, thus promoting the de-ethylation process and accounting for the higher de-ethylation rate of RhB over the ZP/AgCl physical mixture with respect to that observed over the pure AgCl sample. The electron injection is reasonably further favoured in the ZP/AgCl composites, where a more intimate contact between ZP and AgCl is expected with respect to the physical mixture, thus leading to a best catalytic activity.

Finally, it has also been reported by Merka *et al.*[17c] that photodegradation of RhB resulted to be enhanced in acidic media, since it can be assumed that low pH values lead to a higher concentration of photogenerated oxidants and/or to the formation of different oxidative species having higher oxidation potentials. These pH-dependent oxidative species may influence the direct photodegradation of RhB in the solution bulk. By taking into account that the pH of a suspension, consisting of 30 mg of nanosized ZP in 25 mL of water, is ≤ 3, it is reasonable to infer that, in the presence of ZP, the pH of the solution is low enough to promote the formation of oxidative species which lead to a more efficient direct photodegradation of RhB in the solution bulk.

3.5 Catalyst recyclability

The catalytic activity of the best composite photocatalyst, ZP/*1.16*AgCl has been tested for three consecutive catalytic experiments and the evolution of the RhB adsorption spectrum during time is shown in the Supporting Information (Figure S2). The percentages of chromophore cleavage for the second and third cycle, reported in Table 3, show that the composite catalyst keeps its catalytic activity almost unchanged after three catalytic cycles. The X-ray powder pattern of the sample after three cycles (Figure S3) shows the typical peaks of the ZP and cubic AgCl phases, together with weak reflections which could be assigned to metallic Ag.

Moreover, the ZP/AgCl mass ratio for the ZP/*1.16* AgCl composite, determined by X-ray analysis, goes from 1.98 for the fresh sample, to 2.55 after three cycle usage: this difference can be attributed both to the further reduction of the Ag^+ ions of the AgCl lattice to Ag(0) and/or to a partial leaching

of AgCl particles during the photocatalytic tests. However, it is noteworthy that the activity of the ZP/*1.16* AgCl composite after three cycles is significantly higher than that of fresh AgCl.

4 Conclusions

A new class of composite photocatalysts, based on α-type zirconium phosphate and AgCl (ZP/*x*AgCl), was prepared by reaction of hydrochloric acid with silver exchanged layered zirconium phosphate samples, having composition $Zr(AgPO_4)_x(HPO_4)_{2-x}$, with x= 0.28, 0.56, 1.16. The X-ray powder diffraction patterns of the composite photocatalysts ZP/*x*AgCl (x = 0.28, 0.56, 1.16), show the typical reflections of the α-$ZP{\cdot}H_2O$ phase and those of the cubic AgCl phase, with an average crystalline domain size in the range 270-400 nm. Scanning electron microscopy analysis revealed that the ZP/*x*AgCl composites consist of AgCl particles with size ≤ 1 μm, while UV-Vis diffuse reflectance spectroscopy proved that ZP/*x*AgCl is effectively converted in ZP/*x*(Ag@AgCl) after few minutes of irradiation with the same halogen lamp used for the photocatalytic tests. The photocatalytic activities of the ZP/*x*AgCl composites were tested in the degradation of Rhodamine B (RhB).

The ZP/*x*AgCl composites turned out to have better catalytic properties than a pure AgCl, with particle size in the range 0.5 ÷ 2 μm, and ZP/*1.16*AgCl resulted to be the best composite photocatalyst. Moreover, ZP/*1.16*AgCl exhibited a high catalytic activity even after three catalytic cycles. The smaller size, in the ZP/*x*AgCl composites, of both AgCl particles and Ag nanoparticles, formed from them upon irradiation, the chemisorption abilities of ZP toward RhB, and the acidic environment produced by ZP, can account for the higher catalytic activity of the composites with respect that of the pure AgCl reference sample.

It is noteworthy that the investigated systems are much more active toward the RhB degradation than similar composites based on Ag@AgCl intercalated in layered $K_4Nb_6O_{17}$, which reached an almost complete RhB degradation in 120 minutes with a 250 W metal halide lamp.[20] The ZP/*x*AgCl

composites result to be also competitive, the experimental conditions being similar, with hybrid systems based on Ag@AgCl and graphene oxide, which caused a 95% of RhB degradation within 16 minutes.[21] Moreover, the investigated composite systems provide a model for the development of similar ZP/AgX composite photocatalysts (X= Br, I), which could be employed for the photodegradation of different classes of potential organic pollutants, such as drugs.

References

1 A. Clearfield, U. Costantino in *Comprehensive supramolecular chemistry, Solid State Supramolecular Chemistry: Two and three-dimensional inorganic networks*, ed. G. Alberti, T. Bein, Pergamon, Oxford: Elsevier Ltd. Press, 1996, vol. 7, ch. 4.

2 A. Clearfield, S. Cheng, *J. Inorg. Nucl. Che.,* 1980, **42**, 1341-1345.

3 B. Tian, J. Zhang, *Catal. Surv. Asia,* 2012, **16**, 210-230.

4 P. Wang, B. Huang, Y. Daia, M.-H. Whangbo, *Phys. Chem. Chem. Phys*., 2012, **14**, 9813-9825.

5 a) Y. Xia, N.J. Halas, *MRS Bull.,* 2005, **30**, 338-348; b) R. Jiang, B. Li , C. Fang, J. Wang, *Adv. Mater.*, 2014, **26**, 5274–5309.

6 a) P. Wang, B. Huang, X. Qin, X. Zhang, Y. Dai, J. Wei, M.-H. Whangbo, *Angew. Chem. Int. Ed.,* 2008, **47**, 7931-7933; b) P. Wang, B. Huang, Z. Lou, X. Zhang, X. Qin, Y. Dai, Z. Zheng, X. Wang, *Chem. Eur. J.,* 2010, **16**, 538-544; c) L. Han, P. Wang, C. Zhu, Y. Zhai, S. Dong, *Nanoscale*, 2011, **3**, 2931-2935.

7 M. Pica, A. Donnadio, D. Capitani, R. Vivani, E. Troni, M. Casciola, *Inorg. Chem*., 2011, **50**, 11623-11630.

8 G. Kortuem in *Reflectance Spectroscopy*, Springer-Verlag, Berlin, Heidelberg, New York, 1969.

9 U. Costantino, A. Isernia, G. De Meo, *Bull. Che. Soc. Jpn*, 1980, **53**, 2384-2388.

10 C. Larson, R. B.Von Dreele in *Generalized Crystal Structure Analysis System*, Los Alamos National Laboratory: Los Alamos, NM, 2001.

11 D. L. Bish, S. A. Howard, *J. Appl. Crystallogr.,* 1998, **21**, 86-91.

12 Y. Tang, Z. Jiang, G. Xing, A. Li, P. D. Kanhere, Y. Zhang, T. C. Sum, S. Li, X. Chen, Z. Dong, Z. Chen, *Adv. Funct. Mater.*, 2013, **23**, 2932-2940.

13 a) D. Chen, S. H. Yoo, Q. Huang, G. Ali, S. O. Cho, *Chem. Eur. J.* 2012, **18**, 5192 – 5200; b) J. Jiang, L. Zhang, *Chem. Eur. J.* 2011, **17**, 3710-3717

14 Q. Xiang, J. Yu, B. Cheng, H. C. Ong, *Chem. Asian. J.*, 2010, **5**, 1466-1474.

15 P. K. Jain, K. S. Lee, I. H. El-Sayed, M. A. El-Sayed, *J. Phys. Chem. B*, 2006, **110**, 7238-7248.

16 T. Watanabe, T.Takizawa, K. Honda, *J. Phys. Chem.*, 1977, **81**, 1845-1851.

17 a) T. Wu, G. Liu, J. Zhao, H. Hidaka, N. Serpone, *J.Phys. Chem. B*, 1998, **102**, 5845-5851; b) X. Li, J. Ye, *J. Phys. Chem. C,* 2007, **111**, 13109-13116; c) O. Merka,V. Yarovyi, D. W. Bahnemann, M. Wark, *J. Phys. Chem. C* 2011, **115**, 8014–8023.

18 H. Tong, S. Ouyang, Y. Bi, N. Umezawa, M. Oshikiri, J. Ye, *Adv. Mater.,* 2012, **24**, 229-251.

19 a) M. G. Bernasconi, M. Casciola, *J. Chromatogr.*, 1980, **195**, 270-276; b) G.G. Aloisi, U. Costantino, F. Elisei, M. Nocchetti, C. Sulli, *Mol. Cryst. Liq. Cryst.* 1998, **311**, 245-250.

20 W. Cui, H. Wang, L. Liu, Y. Liang, J.G. McEvoy, *Appl. Surf. Sci.*, 2013, **283**, 820-827.

21 H. Zhang, X. Fan, X. Quan, S. Chen, H. Yu, *Environ. Sci.Technol.*, 2011, **45**, 5731-5736.

Table of contents

Nanosized zirconium phosphate/AgCl composite materials: a new synergy for an efficient photocatalytic degradation of organic dye pollutants

Monica Pica, Morena Nocchetti, Berardo Ridolfi, Anna Donnadio, Ferdinando Costantino, Pier Luigi Gentili, Mario Casciola.

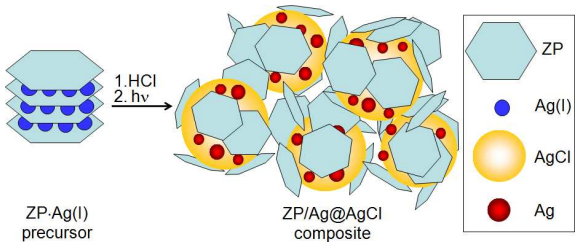

Silver exchanged nanosized zirconium phosphate is used as source of Ag^+ ions in the preparation of AgCl. The obtained zirconium phosphate/AgCl composites work much better than pure AgCl toward the photoassisted degradation of Rhodamine B.